A HYPERSPECTRAL REMOTE SENSING FUSION TECHNOLOGY BASED ON SPECTRAL NORMALIZATION OF GF AND ZY SERIES SATELLITES

Shuhan Liu[1]， Hongzhou Li[1,*], Xia Wang[1], Changru Liu[1], Yangyang Wang[1], Pengfei Huang[1]

[1] Land Satellite Remote Sensing Application Center, MNR
*Corresponding author, e-mail address: coaqatig@163.com

Commission III, WG III/6

KEY WORDS: Data Fusion, Spectral Normalization, Hyperspectral, GF5, GF1, ZY3

ABSTRACT:

Globalized surface coverage, environmental monitoring and other earth system science and high-quality global surface coverage monitoring applications urgently need basic hyperspectral remote sensing reflectance data to support. Spectral reflectance is the core data product of hyperspectral satellite remote sensing data, which is directly related to the application efficiency and quality of hyperspectral satellite. Due to the differences in spectral range, resolution width, central wavelength and other factors between multispectral and hyperspectral remote sensing images, the fusion processing of hyperspectral and multispectral remote sensing images is extremely difficult. In this study, the idea of normalization of physical parameters is adopted. Based on the remote sensing data of multi-source satellites such as GF5, GF1WFV and ZY3, the physical parameters of GF series satellites are fused to improve the spatial resolution of hyperspectral remote sensing images while the physical parameters of surface parameters are maintained. According to the fusion quality evaluation results of noise, information entropy, clarity, spectral angle cosine, correlation coefficient and root mean square error, the fusion results are consistent with the original numerical performance. The noise level, information entropy and clarity index of GF5 and ZY3 fusion are better. The spectral angle cosine, correlation coefficient and root mean square error index of GF5 and GF1 fusion are better. This study provides a new way and method for high-precision and quantitative processing of hyperspectral remote sensing data.

1. INTRODUCTION

At present, China has GF5, ZY1 - 02D and Orbita high-resolution hyperspectral satellites in orbit. Under the dual drive of the technical guidance of improving the hyperspectral acquisition ability and the application traction of global timing surface coating monitoring, the quantitative fusion of hyperspectral remote sensing has become an urgent technical problem to be solved(Biswas et al., 2015a). The difficulty lies in: First, the correspondence between high-multispectral bands is fuzzy(Song et al., 2020); second, hyperspectral contains multi-dimensional temporal and spatial spectrum information and many error influencing factors(Yang and Jiao, 2008); third, the traditional mathematical fusion model is easy to destroy the essence of hyperspectral quantitative remote sensing(Ghassemian, 2016). The core data product of hyperspectral remote sensing is reflectance(Ma et al., 2021), which realizes the high precision fusion of hyperspectral reflectance under the condition of maintaining the true value of reflectance physical quantity(Peng et al., 2021). On the one hand, it breaks through the high spatial resolution, on the other hand, it improves the accuracy of hyperspectral reflectance(Luo et al., 2016). This study provides important experimental technical support for mining the quantitative ability of hyperspectral remote sensing, improving the accuracy of reflectance and leading the advanced processing and application of hyperspectral remote sensing.

2. METHOD

Spectral normalization model is improved by color normalization algorithm(Cheng et al., 2015). It is an improved algorithm which can be applied to fusion of high spatial resolution image and high spectral resolution image(Cheng et al., 2013). The main idea is to increase the information of remote sensing images with low spatial resolution(Pandit and Bhiwani, 2021) and high spectral resolution according to remote sensing images with high spatial resolution and low spectral resolution(Ma et al., 2020), and keep the value of spectral images unchanged.

The spectral normalization method of hyperspectral fusion is that, firstly, the hyperspectral image is sampled to make it have the same pixel size as the high spatial resolution image. Secondly, the high spatial resolution image is multiplied by the hyperspectral resolution image of each band by pixel(Du et al., 2013). Thirdly, the results obtained by multiplication are normalized to the band average of the wavelength range of the hyperspectral resolution image covered by the high spatial resolution image(Biswas et al., 2015b). Finally, each fused image after spectral normalization is generated. The formula is as follows:

$$SN_i = \left(\frac{HSI_i \cdot HRI}{HSI_p} \right) \quad (1)$$

In formula (1), HSI_i represents the low spatial resolution and high spectral resolution image data of the i band. HSI_p represents the average value of all bands of low spatial resolution and high spectral resolution images, HRI represents

* Corresponding author.
E-mail address: coaqatig@163.com (Hongzhou Li)

the high spatial resolution and low spectral resolution image data, SN_i is the corresponding band after spectral normalization.

3. EXPERIMENTS

3.1 Multi resolution remote sensing data

In this study, GF5 hyperspectral images, GF1WFV wide-band multispectral images and ZY3 multispectral images were collected as experimental data. The spatial resolution covers 30 m, 16 m and 5.8 m. The number of spectral bands includes visible near-red short-wave infrared 330 bands and visible near-infrared 4 bands. The spatial resolution and spectral resolution of remote sensing data are highly representative.

Satellite	Imaging time	Range
GF1	2019.8.21	E 111.42 N34.71
ZY3	2019.9.13	E 111.26 N34.58
GF5	2019.8.08	E 111.63 N34.19
	2019.10.05	E 111.58 N34.62

Table 1. Data list

3.1.1 GF5 satellite: GF5 satellite was launched in 2018, it is the only hyperspectral satellite among the seven civil satellites in the major special project of high-resolution earth observation system. It was the satellite with the largest payload and the highest spectral resolution among the major national high score science and technology projects in that year. It is also an optical remote sensing satellite with the most detection means in China, designed as a solar synchronous orbit with an orbital height of about 705km. For the first time, the satellite carried six loads, including atmospheric trace gas differential absorption spectrometer, atmospheric main greenhouse gas monitor, atmospheric multi angle polarization detector, atmospheric environment infrared very high resolution detector, visible short wave infrared hyperspectral camera and full spectrum imager. The satellite can monitor atmospheric aerosol, dioxide, nitrogen dioxide, carbon dioxide, methane, water bloom, water quality, warm drainage of nuclear power plants, land vegetation, straw incineration, urban heat island and other environmental factors.

Spectral range	0.4-2.5
spatial resolution	30m
width	60km
spectral resolution	VNIR: 5nm SWIR: 10nm

Table 2. Parameters of visible short wave infrared hyperspectral camera

3.1.2 GF1 satellite:
GF1satellite is the first satellite in the major special space-based system of the national high-resolution earth observation system. Its main purpose is to break through the high spatial resolution, optical remote sensing technology combining multispectral and high time resolution, multi load image mosaic and fusion technology, high precision and high stability attitude control technology, key technologies such as high-resolution data processing and application. After the successful launch of GF1 satellite, it can provide high-precision and wide-range space observation services for land and resources departments, agricultural departments, meteorological departments and environmental protection departments. It plays an important role in geographic mapping, marine and climate meteorological observation, water conservancy and forestry resources monitoring, fine urban and transportation management, epidemic assessment and public satellite emergency response, earth system scientific research and other fields.

Parameter	2m resolution panchromatic / 8m resolution multispectral camera		16m resolution multispectral camera
Spectral range	Panchromatic	0.45-0.90 μm	
	Multispectral	0.45-0.52 μm	0.45-0.52 μm
		0.52-0.59 μm	0.52-0.59 μm
		0.63-0.69 μm	0.63-0.69 μm
		0.77-0.89 μm	0.77-0.89 μm
Spatial resolution	Panchromatic	2m	16m
	Multispectral	8m	
Width	60km(2 cameras)		800km(4 cameras)

Table 3. Technical index of GF1 satellite payload

3.1.3 ZY3 satellite: ZY301, ZY302, ZY303 was launched in 2012, 2016 and 2020 respectively. Realize the networking operation of independent civil three-dimensional surveying and mapping, form a business observation constellation, and shorten the revisit cycle and coverage cycle. Give full play to Samsung's efficiency and obtain high-resolution stereo images and multispectral images covering the whole country and even the world in a long-term, continuous, stable and rapid manner. ZY3 series provides a solid foundation for 1:50000 and 1:25000 scale stereoscopic mapping. After the operation of Samsung networking, it will further strengthen the service support capacity of domestic satellite images in land surveying and mapping, resource investigation and monitoring, disaster prevention and mitigation, agriculture, forestry and water conservancy, ecological environment, urban planning and construction, transportation and other fields.

3.2 Selection and overview of research area

The study area is located in Sanmenxia City. Sanmenxia City is located in the southern Golden Triangle of the Yellow River at the junction of Henan, Shanxi and Shaanxi provinces, Tableland, hills and loess are the main landforms,
It belongs to warm temperate continental monsoon semi-arid climate; Sanmenxia City is located on the terrace on the South Bank of the Yellow River. It faces water on three sides and looks like a peninsula. It is known as "surrounded by mountains and water on three sides". Sanmenxia City is located in the west of Henan Province, Between 33 ° 31 ′ 24 ″ ~ 35 ° 05 ′ 48 ″ N and 110 ° 21 ′ 42 ″ ~ 112 ° 01 ′ 24 ″ E, It is located in the southern Golden Triangle of the Yellow River at the junction of Henan, Shanxi and Shaanxi provinces, The climate here is pleasant, with four distinct seasons, and the annual average temperature is 14.2 ℃. The annual rainfall is generally 400 mm - 700 mm. The frost free period is 215 days,
The annual sunshine time is about 2051.6 hours. GF-5 satellite image pixel size 2006 * 2081. GF-1 multispectral image captured by WFV3 camera with pixel size of 12001 × 13403.

Load	Band NO.	Spectral range	Spatial resolution	Width	Side swing ability	revisit time (day)
Forward looking camera	_	0.5-0.8	3.5	52	+/- 32 degree	3-5
Rear view camera	_	0.5-0.8	3.5	52	+/- 32 degree	3-5
Front view camera	_	0.5-0.8	2.1	51	+/- 32 degree	3-5
Multispectral camera	1	0.45-0.52	6	51	+/- 32 degree	5
	2	0.52-0,59				
	3	0.63-0.69				
	4	0.77-0.89				

Table 4. Technical index of ZY3 satellite payload

The pixel size of ZY-3 multispectral image is 8817 × 8789. All image projection coordinate systems are WGS _ 1984.

3.3 Hyperspectral fusion process

Hyperspectral fusion processing. For hyperspectral and multispectral remote sensing data, the applicable band resampling methods are used to maintain the same dimension of hyperspectral and multispectral remote sensing data. After registration and correction, the hyperspectral and multispectral data are accurately registered in space geometry. On this basis, the spectral normalization model studied in this paper is used for fusion processing to generate the fusion results of hyperspectral and multispectral surface reflectance. Figure 1 for detail. The comparison before and after image fusion is shown as follows. Figure 2 for detail.

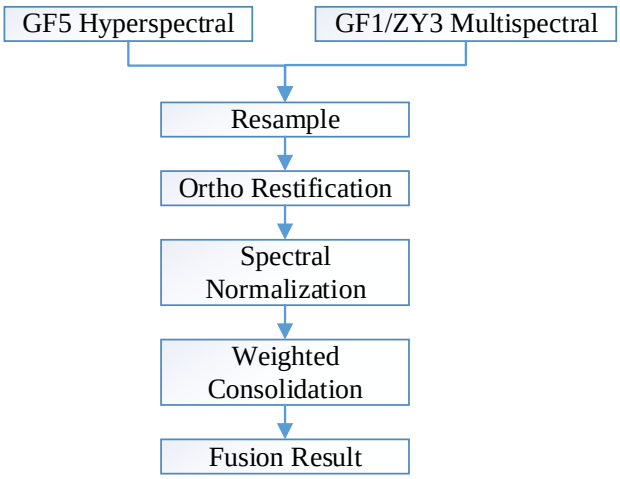

Figure 1. Flow chart of multispectral data and hyperspectral data fusion

(GF5) (GF1) (ZY3) (GF5+GF1) (GF5+ZY3)

Figure 2. Comparison of GF5, GF1, ZY3 fusion image

3.4 Fusion quality evaluation

In this paper, six quantitative indicators including noise, information entropy, clarity, spectral angle cosine, correlate coefficient and root mean square error are used to evaluate the results of hyperspectral reflectance fusion image.

Noise is an important quantitative index to measure the quality of hyperspectral image(Nencini et al., 2007). In this paper, a more stable hyperspectral image noise assessment method. Select the basic characteristics of spectral image ground object homogeneity and spectral dimension high correlation, calculate the hyperspectral noise level. According to Formulas (2) and (3), the residuals in the uniform region of the reflectance image are calculated, and the standard deviation of the residuals is taken as the standard deviation of the noise. The smaller the average value of noise standard deviation is, the higher the proportion of effective information in the image is, and the better the image quality is.

$$\mathrm{r}_{i,j,k} = x_{i,j,k} - \hat{x}_{i,j,k} \tag{2}$$

In formula (2), $\mathrm{x}_{i,j,k}$ is the observed value, $\hat{\mathrm{x}}_{i,j,k}$ is the estimation of $x_{i,j,k}$, which can be estimated by multiple linear regression method.

$$\hat{\mathrm{x}}_{i,j,k} = a + bx_{i,j,k-1} + cx_{i,j,k+1} + dx_{p,k} \tag{3}$$

In formula (3), p represents the spatial neighborhood pixel of $x_{i,j,k}$ and a,b,c,d is the coefficient of multiple linear regression equation

Information entropy is an important quantitative index to measure the information richness of remote sensing images(Rasti and Ghamisi, 2020). Information entropy is calculated according to formula (4). The higher the information entropy, the higher the information content in the representative image.

$$H(U) = E[-\log p_i] = -\sum_{i=1}^{n} p_i \log p_i \quad (4)$$

i is the possible gray value, P_i is the probability of *i*.

Use the average gradient index as the clarity evaluation index(Yang et al., 2018). The greater the average gradient, the higher the resolution of the image according to formula (5).

$$\nabla \bar{g} = \frac{1}{MN}\sum_{i-1}^{M}\sum_{j=1}^{N}\sqrt{[\frac{\delta f(x_i, y_j)^2}{\delta x_i} + \frac{\delta f(x_i, y_j)^2}{\delta y_j}]} \quad (5)$$

MN is the number of rows and columns of the image, $f(x_i,y_j)$ is the pixel value of the fused image at *(i,j)*.

Spectral angle cosine (SAC) is calculated according to formula (6) which used to measure the similarity between the spectra of hyperspectral reflectance. The smaller the spectral angle is, the higher the similarity is. Compared with the surface reflectance of hyperspectral images, the smaller the spectral angle is, the closer the cosine value is to 1, and the more similar the two spectral curves are

$$SAC(x, y) = \cos^{-1}\frac{\sum_{i-1}^{n} x_i y_i}{\sqrt{\sum_{i=1}^{n} x^2}\cdot\sqrt{\sum_{i=1}^{n} y^2}} \quad (6)$$

x and *y* represent the spectral curve and contrast curve respectively, x_i and y_i represent the spectral value of the *i* band in the curve, and *n* is the number of bands of the image.

Correlation coefficient (CC) is an important quantitative index to measure image similarity and information fidelity. The results range from 0 to 1. The lower the value is, the closer to 0, the worse the spectral curve retention is. The closer to 1, the better the consistency with hyperspectral image information is. The formula is as follows.

$$CC = \frac{\sum_{i=1}^{M}\sum_{j=1}^{N}(M_{i,j} - \bar{M}).(F_{i,j} - \bar{F})}{\sqrt{\sum_{i=1}^{M}\sum_{j=1}^{N}(M_{i,j} - \bar{M})^2.\sum_{i=1}^{M}\sum_{j=1}^{N}(F_{i,j} - \bar{F})^2}} \quad (7)$$

M and *N* are the total number of rows and columns of the image, $M_{i,j}$ and $F_{i,j}$ represent the spectral values of each band in the fused image and hyperspectral image. $\bar{M}$ and $\bar{F}$ represent the average of each band in fused and hyperspectral images.

Root Mean Squared Error (RMSE) represents the square root of observation ratio and deviation square between observed value and true value(Zhang et al., 2020). The RMSE indicates the degree of dispersion between the observed value and the true value. The smaller the RMSE is, the higher the accuracy of the observed value is, and the smaller the difference between the spectral curves is, indicating that the closer the reference spectrum is. The formula is as follows.

$$RMSE = \sqrt{\frac{\sum_{i=1}^{M}\sum_{j=1}^{N}[R(i, j) - F(i, j)]^2}{MN}} \quad (8)$$

In formula (7), *R(i,j)* and *F(i,j)* represent the spectral reflectance of fused image and reference image in *(i,j)* pixel, respectively. *M* and *N* are the total number of rows and columns of the image.

4. RESULTS

In this paper, three commonly used image quality evaluation indicators, noise level, information entropy (IE) and clarity(Jinju et al., 2019) are used for evaluation of image quality before and after fusion (Table 1)

	Noise	IE	Clarity
GF5	23.7953	7.6894	102.8529
GF1	16.5768	6.8768	125.9518
ZY3	22.4894	7.8975	148.4831
GF5+GF1	23.6514	7.5107	109.4823
GF5+ZY3	23.3287	7.9263	130.8295

Table 5. Image quality evaluation before and after fusion

The results show that the fusion effect of GF5 and ZY3 is better than that of GF5 and GF1. The noise level, information entropy (IE) and clarity after the fusion of GF5 and ZY3 are 23.3287, 7.9263 and 130.8295, respectively. The noise level, information entropy (IE) and clarity after the fusion of GF5 and GF1 are 23.6514, 7.5107 and 109.4823, respectively.

Select typical feature roads to calculate spectral angle cosine, correlation coefficient and root mean square error for quality evaluation. The results are shown in Table 2.

The results show that in the VNIR spectrum, the spectral angle chord and correlation coefficient of the fusion results of GF5 and GF1 are 0.9852 and 0.9361, respectively. The spectral angle chord and correlation coefficient of fusion results of GF5 and ZY3 are 0.9836 and 0.8704, respectively. GF5 and GF1 fusion results are better. In the SWIR spectrum, the spectral angle chord and correlation coefficient of the fusion results are 1, and the root mean square error is 0. The fusion results are consistent with the original GF5 reflectance. In the Full spectrum, the spectral angle cosine, correlation coefficient and RMSE of the fusion results of GF5 and GF1 are 0.9868, 0.9875 and 0.0185, respectively. The spectral angle cosine, correlation coefficient and RMSE of fusion results of GF5 and ZY3 are 0.9875, 0.9863 and 0.0269, respectively. GF5 and GF1 fusion results are better.

The results show that in the VNIR spectrum, the spectral angle chord and correlation coefficient of the fusion results of GF5 and GF1 are 0.9852 and 0.9361, respectively. The spectral angle chord and correlation coefficient of fusion results of GF5 and ZY3 are 0.9836 and 0.8704, respectively. GF5 and GF1 fusion results are better. In the SWIR spectrum, the spectral angle chord and correlation coefficient of the fusion results are 1, and the root mean square error is 0. The fusion results are consistent with the original GF5 reflectance. In the Full spectrum, the spectral angle cosine, correlation coefficient and RMSE of the fusion results of GF5 and GF1 are 0.9868, 0.9875 and 0.0185, respectively. The spectral angle cosine, correlation coefficient and RMSE of fusion results of GF5 and ZY3 are 0.9875, 0.9863 and 0.0269, respectively. GF5 and GF1 fusion results are better.

Typical feature (road)	SAC	CC	RMSE
GF5(VNIR)+GF1	0.9852	0.9361	0.0194
GF5(SWIR)+GF1	1	1	0
GF5(Full Spectrum)+GF1	0.9868	0.9875	0.0185
GF5(VNIR)+ZY3	0.9836	0.8704	0.0393
GF5(SWIR)+ZY3	1	1	0
GF5(Full Spectrum)+ZY3	0.9875	0.9863	0.0269

Table 6. Spectral quality evaluation after fusion

5. CONCLUSIONS

This paper studies hyperspectral remote sensing reflectance fusion processing technology. The hyperspectral data of GF5 and multispectral data of GF1WFV and ZY3 were physically fused by spectral normalization model, and the fusion results were comprehensively evaluated by six quantitative indexes. The results show that the hyperspectral fusion method based on spectral normalization is suitable for the fusion of hyperspectral and multispectral remote sensing information of GF series satellites. The noise level, information entropy and clarity index of GF5 and ZY3 fusion are better, and the spectral angle chord and correlation coefficient index of GF5 and GF1 fusion are better. The hyperspectral remote sensing fusion processing method based on spectral normalization studied in this paper can be further optimized and improved by the spatial resolution, spectral band width, central wavelength and other indicators of fusion processing. It can be applied to the information fusion and quality improvement of hyperspectral and optical remote sensing images, and improve the application effect of hyperspectral remote sensing data.

6. REFERENCES

Biswas, B., Dey, K. N., and Chakrabarti, A.: Remote Sensing Image Fusion using Multithreshold Otsu Method in Shearlet Domain, Procedia Computer Science, 57, 554-562, https://doi.org/10.1016/j.procs.2015.07.388, 2015a.

Biswas, B., Sen, B. K., and Choudhuri, R.: Remote Sensing Image Fusion using PCNN Model Parameter Estimation by Gamma Distribution in Shearlet Domain, Procedia Computer Science, 70, 304-310, https://doi.org/10.1016/j.procs.2015.10.098, 2015b.

Cheng, J., Liu, H., Liu, T., Wang, F., and Li, H.: Remote sensing image fusion via wavelet transform and sparse representation, ISPRS Journal of Photogrammetry and Remote Sensing, 104, 158-173, https://doi.org/10.1016/j.isprsjprs.2015.02.015, 2015.

Cheng, S., Qiguang, M., and Pengfei, X.: A novel algorithm of remote sensing image fusion based on Shearlets and PCNN, Neurocomputing, 117, 47-53, https://doi.org/10.1016/j.neucom.2012.10.025, 2013.

Du, P., Liu, S., Xia, J., and Zhao, Y.: Informatio
n fusion techniques for change detection from multi-temporal remote sensing images, Information Fusion, 14, 19-27, https://doi.org/10.1016/j.inffus.2012.05.003, 2013.

Ghassemian, H.: A review of remote sensing image fusion methods, Information Fusion, 32, 75-89, https://doi.org/10.1016/j.inffus.2016.03.003, 2016.

Jinju, J., Santhi, N., Ramar, K., and Sathya Bama, B.: Spatial frequency discrete wavelet transform image fusion technique for remote sensing applications, Engineering Science and Technology, an International Journal, 22, 715-726, https://doi.org/10.1016/j.jestch.2019.01.004, 2019.

Luo, X., Zhang, Z., and Wu, X.: A novel algorithm of remote sensing image fusion based on shift-invariant Shearlet transform and regional selection, AEU - International Journal of Electronics and Communications, 70, 186-197, https://doi.org/10.1016/j.aeue.2015.11.004, 2016.

Ma, J., Yu, W., Chen, C., Liang, P., Guo, X., and Jiang, J.: Pan-GAN: An unsupervised pan-sharpening method for remote sensing image fusion, Information Fusion, 62, 110-120, https://doi.org/10.1016/j.inffus.2020.04.006, 2020.

Ma, Y., Wei, J., Tang, W., and Tang, R.: Explicit and stepwise models for spatiotemporal fusion of remote sensing images with deep neural networks, International Journal of Applied Earth Observation and Geoinformation, 105, 102611, https://doi.org/10.1016/j.jag.2021.102611, 2021.

Nencini, F., Garzelli, A., Baronti, S., and Alparone, L.: Remote sensing image fusion using the curvelet transform, Information Fusion, 8, 143-156, https://doi.org/10.1016/j.inffus.2006.02.001, 2007.

Pandit, V. R. and Bhiwani, R. J.: Morphology-based spatial filtering for efficiency enhancement of remote sensing image fusion, Computers & Electrical Engineering, 89, 106945, https://doi.org/10.1016/j.compeleceng.2020.106945, 2021.

Peng, Y., Li, W., Luo, X., Du, J., Gan, Y., and Gao, X.: Integrated fusion framework based on semicoupled sparse tensor factorization for spatio-temporal–spectral fusion of remote sensing images, Information Fusion, 65, 21-36, https://doi.org/10.1016/j.inffus.2020.08.013, 2021.

Rasti, B. and Ghamisi, P.: Remote sensing image classification using subspace sensor fusion, Information Fusion, 64, 121-130, https://doi.org/10.1016/j.inffus.2020.07.002, 2020.

Song, Z., Zhang, Z., Yang, S., Ding, D., and Ning, J.: Identifying sunflower lodging based on image fusion and deep semantic segmentation with UAV remote sensing imaging, Computers and Electronics in Agriculture, 179, 105812, https://doi.org/10.1016/j.compag.2020.105812, 2020.

Yang, X.-H. and Jiao, L.-C.: Fusion Algorithm for Remote Sensing Images Based on Nonsubsampled Contourlet Transform, Acta Automatica Sinica, 34, 274-281, https://doi.org/10.3724/SP.J.1004.2008.00274, 2008.

Yang, Z., Mu, X.-d., and Zhao, F.-a.: Scene classification of remote sensing image based on deep network and multi-scale features fusion, Optik, 171, 287-293, https://doi.org/10.1016/j.ijleo.2018.06.024, 2018.

Zhang, C., Yue, P., Tapete, D., Jiang, L., Shangguan, B., Huang, L., and Liu, G.: A deeply supervised image fusion network for change detection in high resolution bi-temporal remote sensing images, ISPRS Journal of Photogrammetry and Remote Sensing, 166, 183-200, https://doi.org/10.1016/j.isprsjprs.2020.06.003, 2020.